Ultrafast Surface State Spin-Carrier Dynamics in the Topological Insulator Bi_{2}Te_{2}Se

Vasudevan Iyer, Yong P. Chen, and Xianfan Xu

Phys. Rev. Lett. **121**, 026807 — Published 11 July 2018

DOI: 10.1103/PhysRevLett.121.026807

Ultrafast Surface State Spin-Carrier Dynamics in Topological Insulator Bi_2Te_2Se

Vasudevan Iyer[1], Yong P Chen[2], and Xianfan Xu[1]*

[1]*Department of Mechanical Engineering and Birck Nanotechnology Center, Purdue University, West Lafayette, 47907, USA*

[2]*Department of Physics and Astronomy and School of Electrical and Computer Engineering and Birck Nanotechnology Center and Purdue Quantum Center, Purdue University, West Lafayette, 47907, USA*

Abstract

Topological insulators are promising candidates for optically driven spintronic devices because photo-excitation of spin polarized surface states is governed by angular momentum selection rules. We carried out femtosecond mid-infrared spectroscopy on thin films of the topological insulator Bi_2Te_2Se, which has higher surface state conductivity compared to conventionally studied Bi_2Se_3 and Bi_2Te_3. Both charge and spin dynamics were probed utilizing circularly polarized light. With a sub-bandgap excitation, clear helicity dependent dynamics was only observed only in thin (< 20 nm) flakes. On the other hand, such dependence was observed for both thin and thick flakes with above band gap excitation. The helicity dependence is attributed to asymmetric excitation of the Dirac like surface states. The observed long lasting asymmetry over ten picoseconds even at room temperature indicates low backscattering of surface state carriers which can be exploited for spintronic devices.

Topological insulator (TI) surface states possess properties such as spin-momentum locking and backscattering protection [1–5], and high mobility [6–8] which make them suited for spintronics

applications [9,10]. A long spin lifetime ensures that information carried by spin is not lost during device operation [11,12]. Therefore, surface states (SS) protected from backscattering are natural candidates for the task. Furthermore, their high mobility can afford faster switching of devices. The widely studied Dirac states in graphene exhibit long spin diffusion lengths upon electrical injection of spin [13,14]. However, they lack spin-momentum locking which prevents optical injection of spin. On the other hand, circularly polarized light has been shown theoretically [15] and experimentally [16,17] to excite only one branch of the spin-momentum locked surface states in TIs. Optical spin control is thus an alternative to conventional magnetic or electric control of devices [18,19]. It is therefore important to examine the interaction of light with SS and understand the resulting charge carrier and spin dynamics.

The fundamental carrier relaxation dynamics of the Dirac like SS following photoexcitation has been studied using angle-resolved photoemission spectroscopy (ARPES) [20–26], terahertz pump-probe spectroscopy [27,28], photoluminescence spectroscopy [29] and optical pump-probe spectroscopy [30–32]. ARPES utilizes energy windows to independently track relaxation of conduction band, valence band, SS, and the coupling between bulk and SS. Most studies used an above bandgap pump and probe energy with linear polarization resulting in interband transitions along with uniform excitation of both branches of the Dirac cone. There is, however, very limited literature on using circularly polarized light to create asymmetric excitations in the SS and study spin dynamics, which is more relevant to optical spin control. Most of the aforementioned works focused only on charge dynamics. Wang and co-workers studied the spin dynamics in Bi_2Se_3 of the second Dirac cone lying above the bulk conduction band and found sub-picosecond relaxation [33]. Similarly, Hsieh et al observed a sub-picosecond spin relaxation in Bi_2Se_3 using second harmonic probing [32]. Recently, Kuroda and co-workers demonstrated

asymmetric excitation of SS in Sb_2Te_3 lasting a few picoseconds with excitation energy below the band gap [25,26]. Apart from the all optical studies, an opto-electronic approach demonstrated spin lifetime of several picoseconds in Bi_2Se_3 [34].

Compared to widely studied Bi_2Se_3 and Bi_2Te_3, topological insulators Bi_2Te_2Se (BTS) and $BiSbTeSe_2$ have better bulk insulating properties due to the Fermi-level being situated near the middle of the bandgap [35,36]. Hence, we chose BTS for our study and performed all-optical pump and probe measurements to investigate the time scales of charge and spin relaxation. We used obliquely incident, circularly polarized mid-infrared/optical pump (7μm, 0.17 eV and 800 nm, 1.55 eV) to excite both below and above the bandgap (0.3 eV, [37]). The probe was fixed at 7 μm. This avoids probing of interband transitions and allows exclusive study of the photon helicity dependent dynamics of SS.

We first examine transient dynamics with both excitation and probing energies of 0.17 eV (7 μm). Flakes of BTS with thicknesses between 14 and 75 nm were exfoliated on CaF_2. Sample preparation and experimental setup are described in supplementary information, note 1. Figure 1 shows the helicity and thickness dependent dynamics at room temperature. ΔR is the change in reflectance of the probe after pump excitation, i.e. $\Delta R = R_{pump} - R$, where R_{pump} and R are the reflectance with and without pump. LL (left circular pump, left circular probe) corresponds to pump and probe having angular momentum pointing in the same direction with respect to the sample surface and RL (right circular pump, left circular probe) corresponds to their angular momentum in opposite directions. A clear difference between RL and LL lasting for more than 10 ps is observed for 14 and 18 nm samples (Fig 1a and 1b). When the pump and probe have the same helicity, we observe a larger signal amplitude - LL has a larger amplitude than RL. The same trend is observed when changing the helicity of the probe instead of the pump - RR shows

a larger signal than RL (supplementary information, Fig. S1). ΔR/R of both RL and LL are normalized to $|RL|_{max}$. The difference between LL and RL is also plotted as |RL|-|LL|. Furthermore, an exponential fit (¯) can be used to describe the decay of the difference, starting from the point of maximum change. The extracted decay time (τ = 8.2 ps and τ = 12 ps in Fig 1a and 1b) quantifies spin relaxation due to the branch selective excitations which will be discussed later. The measurement was also conducted at 80 K (supplementary information, Fig. S2), but only a slightly greater difference between the RL and LL signals was observed.

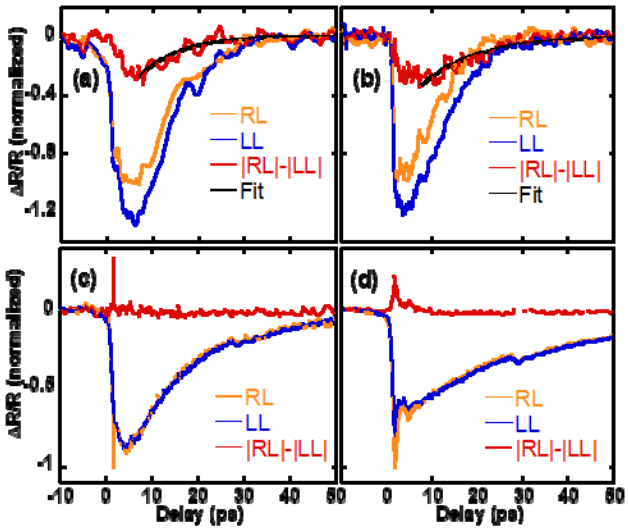

Figure 1: Helicity dependent dynamics for (a) 14 nm (b) 18 nm (c) 45 nm (d) 75 nm flake with 7 μm pump and 7 μm probe. The difference, i.e. |RL|-|LL| vs time, can be fit with an exponential decay time τ = 8.2 ps for (a) and τ = 12 ps for (b).

For thicker samples (Fig. 1c and 1d), only a short lived difference between the reflectance signals RL and LL is observed around time zero. Its origin could be coherent coupling of pump and probe during temporal overlap and hence is not related to SS dynamics. The small bump near 30 ps is due to multiple reflection by the neutral density filter.

The decay time of the reflectivity signal quantifies charge relaxation. The charge decay times for 14 and 18 nm flakes are similar to the values reported for SS relaxation in ARPES studies [20,21], indicating the dynamics observed in the thin flakes is dominated by SS. Theoretically it has been predicted that charge and spin relaxation times should be the same on the Dirac cone of TI [38]. From the experimental data, we see that the time duration when LL and RL are different, which indicates the spin decay time, is the same as the total decay time of the reflectivity signal. Hence, the dynamics is completely dominated by SS in thin flakes. We also noticed the decay dynamics of thin flakes are similar to that of graphene, which has an SS origin. Supplementary information, Fig. S3 shows similar charge decay times for the 14 nm flake and graphene, suggesting a Dirac origin for the BTS flakes.

The slower charge decay as the flakes get thicker is related to atmospheric doping of the samples due to gas adsorption that raises the fermi level [39–43], leading to allowed SS to bulk conduction band transitions and excitations of free carriers. The slow relaxation is thus due to the interband relaxation from the conduction band to SS/valence band, requiring additional scattering mechanisms such as phonon coupling or defect assisted recombination as observed by other researchers [31]. It is reported that bulk samples undergo short term atmospheric doping [42,43] and hence those flakes were likely to have been doped shortly after exfoliation. For our samples, electrical and thermal transport measurements on thin BTS films (< 20 nm) have shown dominating contribution of SS to thermal and electrical conductivity at room temperature as compared to thicker flakes (> 20 nm) [44]. The carrier concentration vs. thickness, along with the Hall measurement [45,46] are shown in supplementary information, Figs. S4-S6, where it can be seen that sub-20 nm flakes have an order of magnitude lower carrier concentration. The obtained carrier concentration of ~ 5×10^{12} cm^{-2} per surface is only half that

obtained from ARPES measurement on thick flake when the Fermi level is located at the bottom of conduction band [39], indicating that the Fermi-level is closer to the charge neutral point. The detailed information on Hall measurements was provided in [44]. Se vacancy migration to the surface and subsequent gas adsorption has been reported as a mechanism for surface doping [47,48]. Thicker films have many quintuple layers behind their surface allowing for vacancy migration and formation of 2D electron gas and subsequent band bending at the surface. Thin flakes on the other hand have fewer migrating sites due to the thinner bulk region and hence do not undergo as much of the surface doping.

We now proceed to explain the helicity dependent dynamics using the band structure in Fig. 2a, which depicts the Fermi-level at 148 meV above the Dirac point as observed in ARPES measurement for freshly cleaved sample in vacuum, not affected by atmospheric doping [39]. RL implies σ+ pump and σ- probe having angular momentum +1 and -1, respectively. We set the spin on the right side branch of SS +1/2 and on the left side -1/2. Hence the in-plane component of a circularly polarized pump (black arrow) at an oblique incidence excites only the depicted transition due to conservation of in-plane angular momentum. Likewise, the circularly polarized probe (orange arrow) at an oblique incidence monitors only the depicted transition. The mid-infrared pump pulses excite electrons from the valence band to the energy levels around the Fermi-energy. In principal, transition from SS to conduction band is also possible. However, the large pool of valence electrons transitioning to SS competes with the SS to conduction band transition, making the latter less probable. The probe, being of the same energy, monitors only SS. Therefore, when probing with the same helicity, the change in reflectance is expected to be larger because $\Delta R \propto \Delta f_1 * \Delta f_2$, where $f_1(k)$ and $f_2(k)$ are momentum dependent Fermi occupation probabilities of the initial and final states. The holes generated in the valence band rapidly (<100

fs) redistribute in k-space making f_1 momentum independent whereas the asymmetrically generated electrons in SS do not redistribute as fast due to the back-scattering protection, making f_2 larger for pumping side of the k-space. Hence the difference in the signals (RL-LL) gives the back-scattering time, which is a net result of many small angle scattering events, and will be discussed in more details later. The difference between the RL and LL in the thin flakes is about 20% of the signal amplitude, which is due to the out-of-plane component of the pump and probe that excite both branches of the Dirac cone simultaneously, giving rise to at least half of the total signal amplitude.

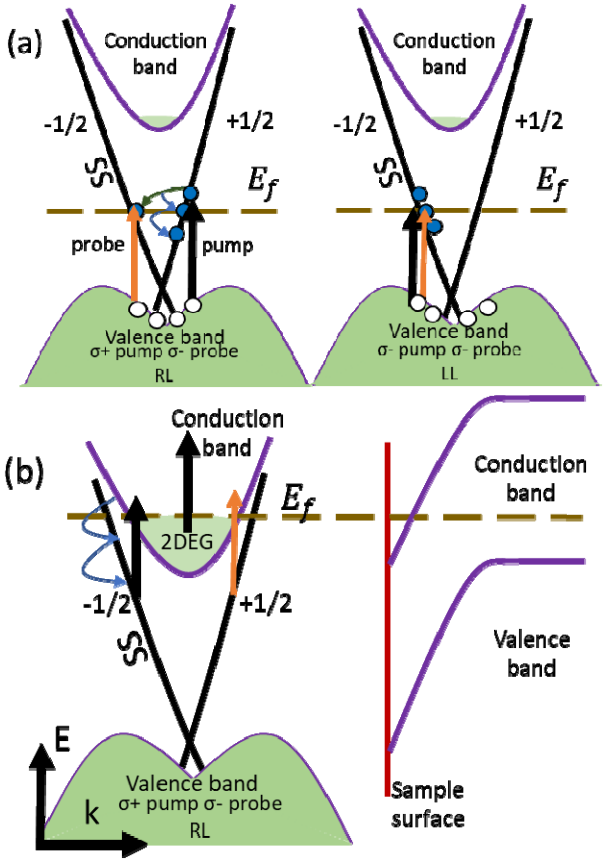

Figure 2: Transition diagram with 7 μm pump and 7 μm probe for (a) thin samples with relatively low Fermi-level. The left figure illustrates σ+ pump and σ- probe (RL), and the right figure σ- pump and σ- probe (LL). LL produces a stronger probe response than RL. (b) Thick

samples with high Fermi-level for σ+ pump and σ- probe (RL), which does not produce a helicity dependent signal (see text). The black arrow represents the pump and the orange arrow represents the probe.

For thicker flakes, the Fermi-level is raised as depicted in Fig. 2b [39]. The SS to conduction band excitation is now possible which leads to interband relaxation and manifests as a slower decay in the signals. An important consideration is the hexagonal warping of the higher energy surface states lying closer to the conduction band, resulting in out-of-plane spin components on an otherwise in-plane spin texture carried by the SS [49–52]. This could be one of the main reasons for the lack of clear helicity dependence in thick flakes owing to excitation of the higher energy portion of the SS. The excitation of 2D gas electrons or defect states is another reason as they do not have a helicity dependence.

We now examine above bandgap excitation. Figure 3 shows flakes of all thicknesses exhibit a helicity dependence, but with reducing magnitude of the difference (|RL|-|LL|) as the flakes become thicker. The difference can be once again fit with an exponential. For the 14 nm flake (Fig. 3a), the total signal decays rapidly, with a spin relaxation time (when RL and LL is different) of 2.8 ps, same as the total signal decay time. The spin relaxation is hence limited by the charge relaxation itself, similar to what is observed with below bandgap excitation (Fig. 1a). It is known that excitation/probing close to the Fermi-level shows a slower decay than excitations away from it due to the requirement of phonons for relaxation [53,54]. This is in good agreement with our observed timescales, since the 800 nm light can excite carriers much above the Fermi-level within the Dirac state, whereas the 7 μm excites carriers in close proximity to the Fermi-level. Here again LL has a larger signal than RL and can be explained using the transition

diagram, Fig. 4a, where electrons are promoted to states near the Fermi-level from deeper lying levels in the valence band. The sharp peak near time zero has been truncated for easier visualization.

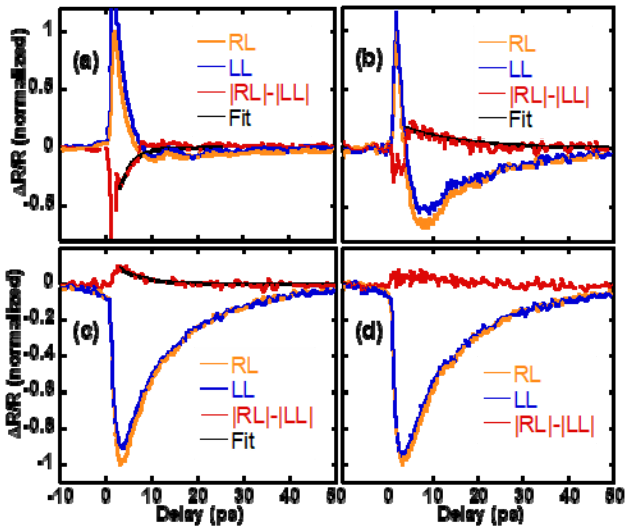

Figure 3: Helicity dependence of (a) 14 nm (b) 18 nm (c) 45 nm and (d) 75 nm sample with 800 nm pump and 7 μm probe. The difference, |RL|-|LL|, is fit with an exponential, τ = 2.8 ps for (a), τ = 12.5 ps for the positive part in (b), and τ = 5.3 ps for (c). The fitting is poor for (d) and hence not shown.

Helicity dependence is also observed for the thicker flakes as shown in Fig. 3c and 3d, which was absent with the 7 μm pump. This is because 800 nm pump can excite almost all energy levels on SS, unlike the 7 μm pump, as illustrated in the transition diagram Fig. 4b. Moreover, RL has a larger signal amplitude, whereas in the 7 μm and 800 nm case for thin flakes, LL has a larger amplitude. This can be explained based on Fig. 4b. The allowed excitation for 800 nm pump is reversed when the Fermi-level is higher, because the initial state is now SS instead of the valence band. For example, a σ+ pump must excite electrons from the -1/2 branch of SS and

result in +1/2 spin electrons in the conduction band (Δ = ½-(-½) = 1). This means electrons from the left side (-1/2) branch are preferentially depopulated by the right circular (σ+) pump, but the left circular probe (σ-) interrogates the left branch, thereby giving a larger signal magnitude. The obtained spin relaxation time is 5.3 ps for the 45 nm sample, but a spin relaxation time is not obtained for the 75 nm sample due to the very low differential signal. It is also not surprising to observe a charge decay time of close to 50 ps, which is similar to that for thick samples when pumped with 7 μm light. This leads to the conclusion that the bulk states continuously feed the surface states and relax via this channel as observed in literature [18,29].

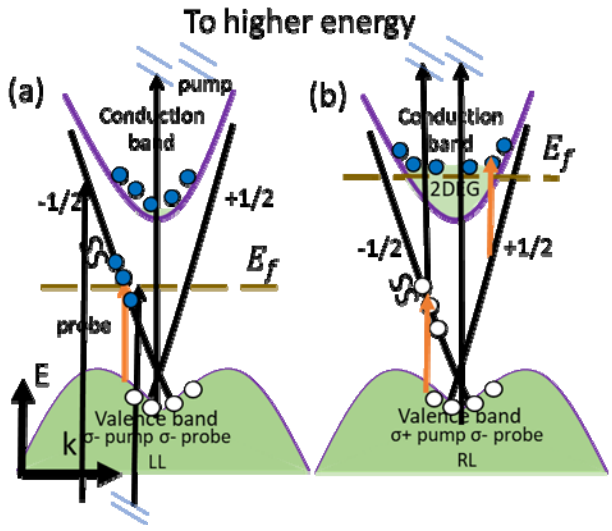

Figure 4: Transition diagram for 800 nm pump and 7 μm probe for (a) thin samples with low Fermi-level for σ- pump and σ- probe (LL), resulting in a stronger probe response for LL, (b) thick samples with high Fermi-level, where RL has a stronger probe response (see text). The black arrow is the pump and orange arrow is the probe.

We now examine the data of the 18 nm flake, Fig. 3b. We see that it shows features possessed by both 14 nm and 45/75 nm flakes, i.e. a negative and positive difference between RL

and LL (τ = 12.5 ps). This, along with the diminishing difference (|RL|-|LL|, Fig. 3a-d) with thickness is an indicator of enhanced surface to bulk coupling as the flakes get thicker. A rapid flow of electrons and holes from the deeper layers towards the surface and subsequent relaxation through the Dirac states is a possible mechanism that reconciles the observation. That is, the influx of unpolarized carriers would diminish the signal difference and at the same time those carriers would account for interband relaxation, which leads to slower relaxation. The 18 nm flake shows similar spin-relaxation timescale with 7 μm and 800 nm excitation because the expected faster relaxation (e.g. 14 nm flake) is offset by the bulk contribution in the latter case, prolonging the carrier lifetime. The influx of carriers could also explain the faster spin relaxation in the 45 nm flake (5.3 ps).

Another important aspect regarding the thickness dependent spin and charge dynamics is small angle scattering of electrons due to phonons. SS electrons in 3D topological insulators are only forbidden from 180° backscattering in the k-space, but can undergo small angle scattering [3]. SS electrons in the very thin samples have little access to scattering with bulk phonons, resulting in reduced small angle scattering, and thus competing charge and spin relaxation is observed in our experiments (Fig 1a, 1b, 3a). In contrast, thick samples can supply phonons and allow for faster decoherence of the SS electrons. This mechanism is in parallel to the influx of unpolarized carriers discussed previously.

SS has been shown to have long mean free paths for charge and spin diffusion to be as much as 2 μm [55–57]. A few metals also have spin diffusion lengths of 100 nm or more [58]. With asymmetry lasting more than 10 ps and a Fermi velocity of $1x10^5$ m/s [39], we estimate a spin diffusion length longer than 1 μm in our samples. This is in reasonable agreement with aforementioned literature, especially for doping compensated materials. A perfectly tuned Fermi-

level in BTS shows SS population lasting as long as 6 μs [59,60]. Hence, BTS can be promising for spintronics. Also, spin relaxation times obtained in this work are comparable to valley depolarization times of few picoseconds observed in valley non-degenerate transition metal dichalcogenides (TMDs) [61–63]. However, due to the massless nature of the Dirac like fermions in TIs, we can expect them to perform comparable to or better than TMDs in spintronics.

In summary, we carried out oblique incidence, helicity resolved optical pump-probe spectroscopy on topological insulator Bi_2Te_2Se using below/above band gap excitation and shown that this technique is useful to study spin dynamics in topological insulators. With below bandgap excitation, a clear helicity dependence was observed for flakes thinner than 20 nm. The vanishing helicity dependence in thick samples was attributed to formation of 2D electron gas on the surface due to gas adsorption at vacancy sites. Above bandgap excitation resulted in asymmetric excitation of surface states for both thin and thick samples. The polarization resolved dynamics reveals the helical spin texture of the surface states and spin relaxation times in the 5-15 ps range, which translates to μm spin diffusion length. Excitations with mid-infrared circularly polarized light is therefore a possible route to control spintronic devices involving thin film topological insulators.

The authors would like to thank Andres Llascahuanga for providing the graphene sample, Anurup Datta for help with AFM measurements, and Dr. Jifa Tian for the Hall measurements. We would also like to thank Ireneusz Miotkowski for synthesizing the Bi_2Te_2Se crystals. Funding from the National Science Foundation (EFMA-1641101) is gratefully acknowledged.

The authors declare no competing financial interests.

References

[1] L. Fu and C. L. Kane, Phys. Rev. B - Condens. Matter Mater. Phys. **76**, 045302 (2007).

[2] Y. Xia, D. Qian, D. Hsieh, L. Wray, A. Pal, H. Lin, A. Bansil, D. Grauer, Y. S. Hor, R. J. Cava, and M. Z. Hasan, Nat. Phys. **5**, 398 (2009).

[3] P. Roushan, J. Seo, C. V Parker, Y. S. Hor, D. Hsieh, D. Qian, A. Richardella, M. Z. Hasan, R. J. Cava, and A. Yazdani, Nature **460**, 1106 (2009).

[4] T. Zhang, P. Cheng, X. Chen, J. F. Jia, X. C. Ma, K. He, L. L. Wang, H. J. Zhang, X. Dai, Z. Fang, X. C. Xie, and Q. K. Xue, Phys. Rev. Lett. **103**, 266803 (2009).

[5] J. F. Tian, I. Miotkowski, S. Hong, and Y. P. Chen, Sci. Rep. **5**, 14293 (2015).

[6] J. G. Checkelsky, Y. S. Hor, R. J. Cava, and N. P. Ong, Phys. Rev. Lett. **106**, 196801 (2011).

[7] N. Koirala, M. Brahlek, M. Salehi, L. Wu, J. X. Dai, J. Waugh, T. Nummy, M. G. Han, J. Moon, Y. M. Zhu, D. Dessau, W. D. Wu, N. P. Armitage, and S. Oh, Nano Lett. **15**, 8245 (2015).

[8] N. P. Butch, K. Kirshenbaum, P. Syers, A. B. Sushkov, G. S. Jenkins, H. D. Drew, and J. Paglione, Phys. Rev. B **81**, 241301 (2010).

[9] Y. Q. Huang, Y. X. Song, S. M. Wang, I. A. Buyanova, and W. M. Chen, Nat. Commun. **8**, 15401 (2017).

[10] A. A. Baker, A. I. Figueroa, L. J. Collins-McIntyre, G. van der Laan, and T. Hesjedal, Sci. Rep. **5**, 7907 (2015).

[11] P. Chuang, S.-C. Ho, L. W. Smith, F. Sfigakis, M. Pepper, C.-H. Chen, J.-C. Fan, J. P. Griffiths, I. Farrer, H. E. Beere, G. A. C. Jones, D. A. Ritchie, and T.-M. Chen, Nat. Nanotechnol. **10**, 35 (2014).

[12] Y. G. Semenov, K. W. Kim, and J. M. Zavada, Appl. Phys. Lett. **91**, 153105 (2007).

[13] C. C. Lin, A. V Penumatcha, Y. F. Gao, V. Q. Diep, J. Appenzeller, and Z. H. Chen, Nano Lett. **13**, 5177 (2013).

[14] P. J. Zomer, M. H. D. Guimaraes, N. Tombros, and B. J. van Wees, Phys. Rev. B **86**, 161416(R) (2012).

[15] P. Hosur, Phys. Rev. B **83**, 035309 (2011).

[16] M. R. Scholz, J. Sanchez-Barriga, J. Braun, D. Marchenko, A. Varykhalov, M. Lindroos, Y. J. Wang, H. Lin, A. Bansil, J. Minar, H. Ebert, A. Volykhov, L. V Yashina, and O. Rader, Phys. Rev. Lett. **110**, 216801 (2013).

[17] M. Xia, J. Jiang, Z. R. Ye, Y. H. Wang, Y. Zhang, S. D. Chen, X. H. Niu, D. F. Xu, F. Chen, X. H. Chen, B. P. Xie, T. Zhang, and D. L. Feng, Sci. Rep. **4**, 5999 (2014).

[18] J. H. Han, A. Richardella, S. A. Siddiqui, J. Finley, N. Samarth, and L. Q. Liu, Phys. Rev. Lett. **119**, 077702 (2017).

[19] Y. Wang, D. P. Zhu, Y. Wu, Y. M. Yang, J. W. Yu, R. Ramaswamy, R. Mishra, S. Y. Shi, M. Elyasi, K. L. Teo, Y. H. Wu, and H. Yang, Nat. Commun. **8**, 1364 (2017).

[20] J. A. Sobota, S. Yang, J. G. Analytis, Y. L. Chen, I. R. Fisher, P. S. Kirchmann, and Z. X. Shen, Phys. Rev. Lett. **108**, 117403 (2012).

[21] Y. H. Wang, D. Hsieh, E. J. Sie, H. Steinberg, D. R. Gardner, Y. S. Lee, P. Jarillo-Herrero, and N. Gedik, Phys. Rev. Lett. **109**, 127401 (2012).

[22] S. Souma, K. Kosaka, T. Sato, M. Komatsu, A. Takayama, T. Takahashi, M. Kriener, K. Segawa, and Y. Ando, Phys. Rev. Lett. **106**, 216803 (2011).

[23] A. Crepaldi, B. Ressel, F. Cilento, M. Zacchigna, C. Grazioli, H. Berger, P. Bugnon, K. Kern, M. Grioni, and F. Parmigiani, Phys. Rev. B **86**, 205133 (2012).

[24] J. Sanchez-Barriga, E. Golias, A. Varykhalov, J. Braun, L. V Yashina, R. Schumann, J.

Minar, H. Ebert, O. Kornilov, and O. Rader, Phys. Rev. B **93**, 155426 (2016).

[25] K. Kuroda, J. Reimann, J. Gudde, and U. Hofer, Phys. Rev. Lett. **116**, 076801 (2016).

[26] K. Kuroda, J. Reimann, K. A. Kokh, O. E. Tereshchenko, A. Kimura, J. Gudde, and U. Hofer, Phys. Rev. B **95**, 081103(R) (2017).

[27] R. V Aguilar, J. Qi, M. Brahlek, N. Bansal, A. Azad, J. Bowlan, S. Oh, A. J. Taylor, R. P. Prasankumar, and D. A. Yarotski, Appl. Phys. Lett. **106**, 011901 (2015).

[28] S. Sim, M. Brahlek, N. Koirala, S. Cha, S. Oh, and H. Choi, Phys. Rev. B **89**, 165137 (2014).

[29] S. Y. Maezawa, H. Watanabe, M. Takeda, K. Kuroda, T. Someya, I. Matsuda, and T. Suemoto, Sci. Rep. **5**, 16443 (2015).

[30] A. Q. Wu, X. Xu, and R. Venkatasubramanian, Appl. Phys. Lett. **92**, 011108 (2008).

[31] C. W. Luo, H. J. Wang, S. A. Ku, H. J. Chen, T. T. Yeh, J. Y. Lin, K. H. Wu, J. Y. Juang, B. L. Young, T. Kobayashi, C. M. Cheng, C. H. Chen, K. D. Tsuei, R. Sankar, F. C. Chou, K. A. Kokh, O. E. Tereshchenko, E. V Chulkov, Y. M. Andreev, and G. D. Gu, Nano Lett. **13**, 5797 (2013).

[32] D. Hsieh, F. Mahmood, J. W. McIver, D. R. Gardner, Y. S. Lee, and N. Gedik, Phys. Rev. Lett. **107**, 077401 (2011).

[33] M. C. Wang, S. Qiao, Z. Jiang, S. N. Luo, and J. Qi, Phys. Rev. Lett. **116**, 036601 (2016).

[34] C. Kastl, C. Karnetzky, H. Karl, and A. W. Holleitner, Nat. Commun. **6**, 6617 (2015).

[35] Y. Xu, I. Miotkowski, C. Liu, J. F. Tian, H. Nam, N. Alidoust, J. N. Hu, C. K. Shih, M. Z. Hasan, and Y. P. Chen, Nat. Phys. **10**, 956 (2014).

[36] Z. Ren, A. A. Taskin, S. Sasaki, K. Segawa, and Y. Ando, Phys. Rev. B **82**, 241306(R) (2010).

[37] A. Akrap, M. Tran, A. Ubaldini, J. Teyssier, E. Giannini, D. van der Marel, P. Lerch, and C. C. Homes, Phys. Rev. B **86**, 235207 (2012).

[38] X. Liu and J. Sinova, Phys. Rev. Lett. **111**, 166801 (2013).

[39] H. Cao, C. Liu, J. Tian, and Y. Xu, ArXiv Prepr. ArXiv … (2014).

[40] S. R. Park, W. S. Jung, C. Kim, D. J. Song, S. Kimura, K. D. Lee, and N. Hur, Phys. Rev. B **81**, 041405(R) (2010).

[41] Z. H. Zhu, G. Levy, B. Ludbrook, C. N. Veenstra, J. A. Rosen, R. Comin, D. Wong, P. Dosanjh, A. Ubaldini, P. Syers, N. P. Butch, J. Paglione, I. S. Elfimov, and A. Damascelli, Phys. Rev. Lett. **107**, 186405 (2011).

[42] C. T. Y. Chen, S. L. He, H. Weng, W. T. Zhang, L. Zhao, H. Y. Liu, X. W. Jia, D. X. Mou, S. Y. Liu, J. F. He, Y. Y. Peng, Y. Feng, Z. J. Xie, G. D. Liu, X. L. Dong, J. Zhang, X. Y. Wang, Q. J. Peng, Z. M. Wang, S. J. Zhang, F. Yang, C. T. Y. Chen, Z. Y. Xu, X. Dai, Z. Fang, and X. J. Zhou, Proc. Natl. Acad. Sci. U. S. A. **109**, 3694 (2012).

[43] M. Bianchi, D. D. Guan, S. N. Bao, J. L. Mi, B. B. Iversen, P. D. C. King, and P. Hofmann, Nat. Commun. **1**, 128 (2010).

[44] Z. Luo, J. Tian, S. Huang, M. Srinivasan, J. Maassen, Y. P. Chen, and X. Xu, ACS Nano **12**, 1120 (2018).

[45] See Supplemental Material [url] for carrier concentration calculation, which includes Ref. [46].

[46] N. W. Ashcroft and D. N. Mermin, *Solid State Physics* (Brooks/Cole, 1976).

[47] D. Hsieh, J. W. McIver, D. H. Torchinsky, D. R. Gardner, Y. S. Lee, and N. Gedik, Phys. Rev. Lett. **106**, 057401 (2011).

[48] D. Hsieh, Y. Xia, D. Qian, L. Wray, J. H. Dil, F. Meier, J. Osterwalder, L. Patthey, J. G.

Checkelsky, N. P. Ong, A. V Fedorov, H. Lin, A. Bansil, D. Grauer, Y. S. Hor, R. J. Cava, and M. Z. Hasan, Nature **460**, 1101 (2009).

[49] L. Fu, Phys. Rev. Lett. **103**, 266801 (2009).

[50] M. S. Bahramy, P. D. C. King, A. de la Torre, J. Chang, M. Shi, L. Patthey, G. Balakrishnan, P. Hofmann, R. Arita, N. Nagaosa, and F. Baumberger, Nat. Commun. **3**, 1159 (2012).

[51] W. Jung, Y. Kim, B. Kim, Y. Koh, C. Kim, M. Matsunami, S. Kimura, M. Arita, K. Shimada, J. H. Han, J. Kim, and B. Cho, Phys. Rev. B **84**, 245435 (2011).

[52] Y. H. Wang, D. Hsieh, D. Pilon, L. Fu, D. R. Gardner, Y. S. Lee, and N. Gedik, Phys. Rev. Lett. **107**, 207602 (2011).

[53] S. Winnerl, M. Orlita, P. Plochocka, P. Kossacki, M. Potemski, T. Winzer, E. Malic, A. Knorr, M. Sprinkle, C. Berger, W. A. De Heer, H. Schneider, and M. Helm, Phys. Rev. Lett. **107**, 237401 (2011).

[54] V. Iyer, P. Ye, and X. Xu, 2D Mater. **4**, (2017).

[55] F. X. Xiu, L. A. He, Y. Wang, L. N. Cheng, L. T. Chang, M. R. Lang, G. A. Huang, X. F. Kou, Y. Zhou, X. W. Jiang, Z. G. Chen, J. Zou, A. Shailos, and K. L. Wang, Nat. Nanotechnol. **6**, 216 (2011).

[56] M. Konig, M. Baenninger, A. G. F. Garcia, N. Harjee, B. L. Pruitt, C. Ames, P. Leubner, C. Brune, H. Buhmann, L. W. Molenkamp, and D. Goldhaber-Gordon, Phys. Rev. X **3**, 021003 (2013).

[57] J. Dufouleur, L. Veyrat, B. Dassonneville, C. Nowka, S. Hampel, P. Leksin, B. Eichler, O. G. Schmidt, B. Buchner, and R. Giraud, Nano Lett. **16**, 6733 (2016).

[58] J. Bass and W. P. Pratt, J. Physics-Condensed Matter **19**, 183201 (2007).

[59] J. Sanchez-Barriga, M. Battiato, E. Golias, A. Varykhalov, L. V Yashina, O. Kornilov, and O. Rader, Appl. Phys. Lett. **110**, 141605 (2017).

[60] M. Neupane, S. Y. Xu, Y. Ishida, S. Jia, B. M. Fregoso, C. Liu, I. Belopolski, G. Bian, N. Alidoust, T. Durakiewicz, V. Galitski, S. Shin, R. J. Cava, and M. Z. Hasan, Phys. Rev. Lett. **115**, 116801 (2015).

[61] C. Mai, A. Barrette, Y. F. Yu, Y. G. Semenov, K. W. Kim, L. Y. Cao, and K. Gundogdu, Nano Lett. **14**, 202 (2014).

[62] F. Mahmood, Z. Alpichshev, Y. H. Lee, J. Kong, and N. Gedik, Nano Lett. **18**, 223 (2018).

[63] R. Schmidt, G. Berghauser, R. Schneider, M. Selig, P. Tonndorf, E. Malic, A. Knorr, S. M. de Vasconcellos, and R. Bratschitsch, Nano Lett. **16**, 2945 (2016).